Comparative Finite Element Simulation of Nonlinear Vibrations and Sensor Output Voltage of Smart Piezolaminated Structures

Ruediger Schmidt and Thang Duy Vu

Abstract—Two geometrically nonlinear plate theories, based either on first- or third-order transverse shear deformation theory are used for finite element modeling and simulation of the transient response of smart structures incorporating piezoelectric layers. In particular the time histories of nonlinear vibrations and sensor voltage output of a thin beam with a piezoelectric patch bonded to the surface due to an applied step force are studied.

Keywords—Nonlinear vibrations, piezoelectric patches, sensor voltage output,. smart structures

I. INTRODUCTION

MODELING and simulation of the geometrically linear and nonlinear static and dynamic response of adaptive structures with integrated distributed control capabilities has attracted considerable research interest in recent years. This paper addresses modeling aspects and finite element simulation of the nonlinear transient vibration response of thin-walled smart structures and of the sensor output voltage of integrated piezoelectric layers or patches.

Numerical simulation of smart piezointegrated thin-walled beam, plate, and shell structures with distributed control capabilities has been performed in many papers in the geometrically linear (see e.g. [1-4]) and geometrically nonlinear [5-13] range of deformation. Typically these structures are very thin and the deformations may exceed the range of validity of linear structural theories (see e.g. [14]). In [5, 8-13] we have shown the importance of geometrically nonlinear analysis, especially when the sensing capabilities of the piezoelectric layers are investigated and for actuation of structures that exhibit stress stiffening effects. In the context of modeling another important issue is the improvement of the linear or nonlinear structural theories on which finite elements are based, especially from the point of view of the adopted kinematical hypothesis. In this paper linear and nonlinear dynamic analysis is performed based on first- and third-order transverse shear deformation plate theory.

Rüdiger Schmidt is with RWTH Aachen University, Germany
e-mail:schmidt@iam.rwth-aachen.de

II. STRAIN-DISPLACEMENT RELATIONS

A. First-order transverse shear deformation plate theory

The results presented in this work, which refer to the first-order transverse shear deformation (FOSD) or Reissner-Mindlin hypothesis, are based on two different types of nonlinearity, namely either on the large deflection von Kármán-type nonlinearity or on the more general nonlinearity associated with the occurrence of moderate rotations. The FOSD hypothesis for the through-thickness variation of the tangential and normal displacement components in the range of validity of these two nonlinear plate theories reads

$$v_\alpha = \overset{0}{v_\alpha} + \Theta^3 \overset{1}{v_\alpha} \quad , \quad v_3 = \overset{0}{v_3} \quad , \tag{1}$$

where the header 0 denotes the mid-surface displacements and the header 1 denotes the rotations at the mid-surface. For a proof that the hypothesis in Eq. (1) is valid in the range of moderate rotations, i.e. up to rotations of at most 10° (but not beyond this range), see [15].

The Green-Lagrange strain components for the nonlinear von Kármán-type FOSD plate theory can be expressed as

$$_0\varepsilon_{\alpha\beta} = \overset{0}{\varepsilon_{\alpha\beta}} + \Theta^3 \overset{1}{\varepsilon_{\alpha\beta}} \quad , \quad _0\varepsilon_{\alpha3} = \overset{0}{\varepsilon_{\alpha3}} \quad , \quad _0\varepsilon_{33} = 0 . \tag{2}$$

The constant terms (denoted by 0), and the linear terms (denoted by 1) are given by

$$\overset{0}{\varepsilon_{\alpha\beta}} = \frac{1}{2}\left(\overset{0}{v_{\alpha|\beta}} + \overset{0}{v_{\beta|\alpha}} + \underline{\overset{0}{v_{3,\alpha}}\,\overset{0}{v_{3,\beta}}} \right) \quad , \quad \overset{1}{\varepsilon_{\alpha\beta}} = \frac{1}{2}\left(\overset{1}{v_{\alpha|\beta}} + \overset{1}{v_{\beta|\alpha}} \right) \quad ,$$

$$\overset{0}{\varepsilon_{\alpha3}} = \frac{1}{2}\left(\overset{0}{v_{3,\alpha}} + \overset{1}{v_\alpha} \right), \tag{3}$$

where the nonlinear terms are marked by a solid line.

The strain-displacement relations for the simulation of the structural behavior in the range of moderate rotations are adopted from the small strain and moderate rotation shell theory of Schmidt and Reddy, see [16, 17].

B. Third-order transverse shear deformation theory

The results referring to the third-order transverse shear deformation theory (TOSD) are obtained with a finite plate element developed in [11, 18] accounting for large deflections in the sense of the von Kármán-type nonlinearity, too. The

TOSD hypothesis for the through-thickness variation of the tangential and normal displacement components reads

$$v_\alpha = \overset{0}{v_\alpha} + \Theta^3 \overset{1}{v_\alpha} + \left(\Theta^3\right)^2 \overset{2}{v_\alpha} + \left(\Theta^3\right)^3 \overset{3}{v_\alpha} \quad , \quad v_3 = \overset{0}{v_3} \quad (4)$$

where the constant, linear, quadratic and cubic terms are denoted by the headers 0, 1, 2 and 3, respectively. If no tangential loads are acting on the upper and lower surfaces, the number of kinematical variables can be reduced from nine in Eq. (4) to only five (like in FOSD theory) and the Green-Lagrange strain components for the TOSD plate element can be expressed as

$$\overset{}{_0\varepsilon_{\alpha\beta}} = \overset{0}{\varepsilon_{\alpha\beta}} + \Theta^3 \overset{1}{\varepsilon_{\alpha\beta}} + \left(\Theta^3\right)^3 \overset{3}{\varepsilon_{\alpha\beta}}, \quad _0\varepsilon_{\alpha 3} = \overset{0}{\varepsilon_{\alpha 3}} + \left(\Theta^3\right)^2 \overset{2}{\varepsilon_{\alpha 3}},$$

$$_0\varepsilon_{33} = 0, \quad (5)$$

where

$$\overset{0}{\varepsilon_{\alpha\beta}} = \frac{1}{2}\left(\overset{0}{v_{\alpha|\beta}} + \overset{0}{v_{\beta|\alpha}} + \underline{\overset{0}{v_{3,\alpha}}\, \overset{0}{v_{3,\beta}}}\right), \quad \overset{1}{\varepsilon_{\alpha\beta}} = \frac{1}{2}\left(\overset{1}{v_{\alpha|\beta}} + \overset{1}{v_{\beta|\alpha}}\right),$$

$$\overset{3}{\varepsilon_{\alpha\beta}} = -\frac{2}{3h^2}\left(\overset{1}{v_{\alpha|\beta}} + \overset{1}{v_{\beta|\alpha}} + 2\overset{0}{v_{3|\alpha\beta}}\right) \quad (6)$$

and

$$\overset{0}{\varepsilon_{\alpha 3}} = \frac{1}{2}\left(\overset{1}{v_\alpha} + \overset{0}{v_{3,\alpha}}\right) \quad , \quad \overset{2}{\varepsilon_{\alpha 3}} = -\frac{2}{h^2}\left(\overset{1}{v_\alpha} + \overset{0}{v_{3,\alpha}}\right) \quad . \quad (7)$$

The cubic terms of the tangential strains (denoted by the header 3) is usually neglected for thin-walled structures.

III. NUMERICAL METHOD

According to the virtual work principle, for a state of equilibrium the internal virtual work δW_i is equal to the external virtual work δW_e. As a continuation of our earlier work[19] in the present paper a total Lagrangian approach is chosen. Consequently, the second Piola-Kirchhoff stress and Green-Lagrange strain tensors are adopted. The electric field vector referring to the undeformed configuration is calculated as the negative gradient of the electric potential Φ along the undeformed surface parameters θ^i as

$$_0 E_i = -\frac{\partial \phi}{\partial \Theta^i} . \quad (9)$$

The mechanical and electrical quantities are coupled to each other by two constitutive equations, namely the direct and the converse piezoelectric effect

$$\{_0 D\} = [e]\{_0\varepsilon\} + [\delta]\{_0 E\} \quad , \quad \{_0 S\} = [c]\{_0\varepsilon\} - [e]^T\{_0 E\},$$

where $\{_0 S\}$ denotes the stress vector, $\{_0\varepsilon\}$ the strain vector, $\{_0 D\}$ the electric displacement vector and $\{_0 E\}$ the electric field vector:

$$\{_0 S\} = \begin{Bmatrix} \sigma^{11} \\ \sigma^{22} \\ \tau^{12} \\ \tau^{23} \\ \tau^{13} \end{Bmatrix}, \quad \{_0\varepsilon\} = \begin{Bmatrix} \varepsilon_{11} \\ \varepsilon_{22} \\ 2\varepsilon_{12} \\ 2\varepsilon_{23} \\ 2\varepsilon_{13} \end{Bmatrix}, \quad \{_0 D\} = \begin{Bmatrix} D^1 \\ D^2 \\ D^3 \end{Bmatrix}, \quad \{_0 E\} = \begin{Bmatrix} E_1 \\ E_2 \\ E_3 \end{Bmatrix}.$$

$$(10)$$

Further $[e] = [d][c]$ and $[e]^T = [c][d]^T$, where $[c]$ denotes the elasticity matrix for anisotropic materials, $[d]$ the piezoelectric constant matrix and $[\delta]$ the dielectric constant matrix:

$$[c] = \begin{bmatrix} c_{11} & c_{12} & c_{13} & 0 & 0 \\ c_{12} & c_{22} & c_{23} & 0 & 0 \\ c_{13} & c_{23} & c_{33} & 0 & 0 \\ 0 & 0 & 0 & c_{44} & c_{45} \\ 0 & 0 & 0 & c_{45} & c_{55} \end{bmatrix}, \quad [d]^T = \begin{bmatrix} 0 & 0 & d_{31} \\ 0 & 0 & d_{31} \\ 0 & 0 & 0 \\ 0 & d_{15} & 0 \\ d_{15} & 0 & 0 \end{bmatrix},$$

$$[\delta] = \begin{bmatrix} \delta_{11} & 0 & 0 \\ 0 & \delta_{22} & 0 \\ 0 & 0 & \delta_{33} \end{bmatrix}. \quad (11)$$

If it is further assumed that the electric field is homogeneously distributed over the electrode pair, only one additional degree of freedom has to be introduced per electrode pair, namely the electric potential. After introducing the principle of virtual work, the differential equations of motion to be solved are

$$[M]\{\ddot{q}\} + \{F_i\} = \{F_e\} \quad , \quad \{Q_i\} = \{Q_e\} \quad (12)$$

where $[M]$ denotes the mass matrix and $\{q\}$ are the generalized nodal displacements. The in-balance nodal force and electrode charge vectors are denoted by $\{F_i\}$ and $\{Q_i\}$, respectively. The externally applied force and charge vectors are denoted by the right subscript e. The electric potentials are calculated from the equilibrium between the mechanically and the electrically induced in-balance charges.

IV. NUMERICAL EXAMPLE

The following numerical example deals with a cantilevered beam consisting of an isotropic master structure with a PZT sensor patch attached 60 mm from the clamping point as depicted in Fig. 1, see also [6, 9]. A step force of 0.6 N is applied at the tip of the beam and the time histories of the transient response (Fig. 2) and sensor output voltage (Fig. 3) are simulated. The step load was chosen such that the maximum rotations occurring in the structure do not exceed the range of moderate rotations. This can be seen in Fig. 4 from the plot of the tip rotations over time.

The material parameters of the beam are $E = 197$ GPa, $v = 0.33$, and $\rho = 7900$ kg/m³, while those of the PZT are $E = 67$ GPa, $v = 0.33$, $\rho = 7800$ kg/m³, $d_{31} = 1.7119 \times 10^{-10}$ m/V, and

$\delta_{33} = 2.03 \ 10^{-8}$ F/m. The present results are obtained with a [10x1] mesh and a time step of $\Delta t = 2 \cdot 10^{-7}$ s.

Fig. 2 and Fig. 3 show the graphs of the tip displacement and of the sensor output voltage, respectively, over time predicted by FOSD and TOSD theory. For linear analysis the results of both theories are identical and confirm those of [9]. In [6] a considerably stiffer response of the beam is predicted. This can be recognized in Fig. 2 by the smaller vibration amplitudes and the higher frequency. It should be mentioned that in [6] a larger step load was applied and that the results of linear analysis presented there were scaled down to the 0.6 N step load applied here.

A step force of 0.6 N, however, results in nonlinear vibrations, just at the limit of the range of moderate rotations (i.e. < 10°), see Fig. 4. In this case still the FOSD and TOSD simulations based on the von Kármán-type nonlinearity (FOSD RVK and TOSD RVK) are identical. Both nonlinear theories predict a slightly stiffer beam response than the linear theories. This can be recognized in Fig. 2 by a decrease of the amplitudes of the tip displacement and an increase of the frequency. The stiffer behavior is explained by the additionally induced membrane stresses near the clamping point, which cannot be predicted by any linear theory. This stress stiffening effect is also visible in the time history of the sensor output voltage in Fig. 3.

A very good agreement is also observed between the predictions of the moderate rotation (FOSD MRT) and von Kármán-type (FOSD RVK and TOSD RVK) theories. Since in the FOSD MRT theory the structural nonlinearity is modeled more accurately, the predicted stress stiffening effect is more pronounced than in the simulations based on the simpler von Kármán-type nonlinearity.

If one compares in Fig. 2 the tip displacements predicted by nonlinear FOSD and TOSD simulations, one recognizes that the FOSD theory predicts a slightly stiffer response than the TOSD theory. This tendency is also visible in the graph of the sensor output voltage over time in Fig. 3.
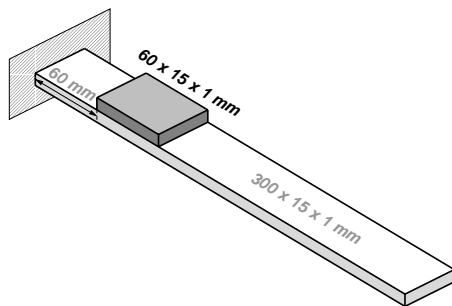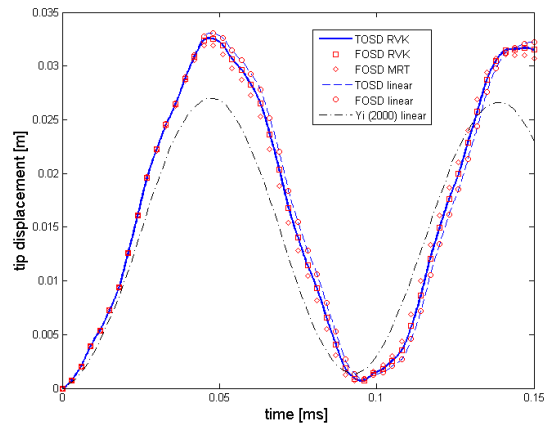

Fig. 2 Time history of the tip displacement of the cantilevered beam loaded by a 0.6 N step force

Fig. 3 Time history of the sensor voltage of the cantilevered beam loaded by a 0.6 N step force

Fig. 1 Cantilevered piezolaminated beam

Fig. 6 Time history of the tip rotation of the cantilevered beam loaded by 0.6 N step force

V. CONCLUSION
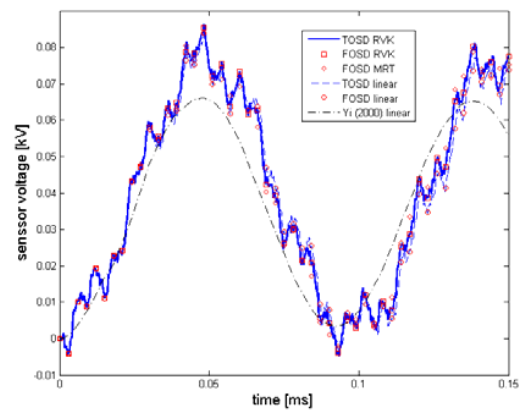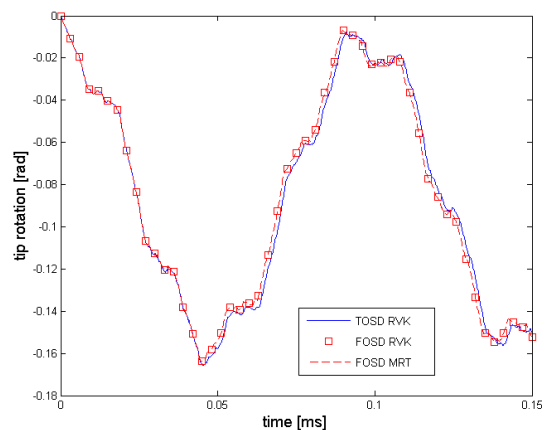
A conclusion section is not required. Although a conclusion may review the main points of the paper, do not replicate the abstract as the conclusion. A conclusion might elaborate on the importance of the work or suggest applications and extensions.

REFERENCES

[1] E.F. Crawley, J. de Luis: Use of piezoelectric actuators as elements of intelligent structures, AIAA Journal 25 (1987), 1373-1385.

[2] R. Lammering: The application of finite shell elements for composites containing piezoelectric polymers in vibration control, Computers & Structures 41 (1991), 1101-1109.

[3] H. Kioua, S. Mirza: Piezoelectric induced bending and twisting of laminated composite shallow shells, Smart. Mater. Struct. 6 (2000), 476-484.

[4] S. Lee, N.S. Goo, H.C. Park, K.J. Yoon, C. Cho: A nine-node assumed strain shell element for analysis of a coupled electromechanical system, Smart. Mater. Struct. 12 (2003), 355-336.

[5] Chróścielewski, P. Klosowski, R. Schmidt: Theory and numerical simulation of nonlinear vibration control of arches with piezoelectric distributed actuators, Machine Dynamics Problems 20 (1998), 73-90.

[6] S. Yi, S.F. Ling, M. Ying: Large deformation finite element analyses of composite structures integrated with piezoelectric sensors and actuators, Finite Elements in Analysis and Design 35 (2000), 1–15.

[7] A. Mukherjee, A.S. Chaudhuri: Piezolaminated beams with large deformations, Int. J. of Solids and Structures 14 (2002), 1567-1582.

[8] S. Lentzen, R. Schmidt: Simulation of sensor application and shape control of piezoelectric structures at large deflections, in *Advances in Computational & Experimental Engineering & Science,* eds. S.N. Atluri, A.J.B Tadeu, p. 439-444, Tech Science Press, 2004.

[9] S. Lentzen, R. Schmidt: A geometrically nonlinear finite element for transient analysis of piezolaminated shells, Proceedings Fifth EUROMECH Nonlinear Dynamics Conference, Eindhoven, The Netherlands, 7 – 12 August 2005, eds. D.H. van Campen, M.D. Lazurko, W.P.J.M. van den Oever, 2492 - 2500, Eindhoven University of Technology 2005.

[10] S. Lentzen, P. Klosowski, R. Schmidt: Geometrically nonlinear finite element simulation of smart piezolaminated plates and shells, Smart Mater. Struct.16 (2007), 2265-2274.

[11] T.D. Vu, S. Lentzen, R. Schmidt: Geometrically nonlinear FE-analysis of piezolaminated plates based on first- and third-order shear deformation theory, Proc. 8th International Conference on Mechatronics Technology, ICMT 2004, Hanoi, Vietnam, 8 – 12 November 2004, eds. Nguyen Khoa Son, Pham Thuong Cat, Pham Anh Tuan, 267-272, Vietnam National University Publisher, Hanoi 2004.

[12] T.D. Vu, R. Schmidt: Nonlinear third-order shear deformation FE simulation of the sensor output voltage of piezolaminated plates, in: "Advances in Computational & Experimental Engineering and Science", eds. W.H. Chen, S.N. Atluri, 452-458, Tech Science Press, Encino, California, USA, 2009.

[13] R. Schmidt, T.D. Vu : Nonlinear dynamic FE simulation of smart piezolaminated structures based on first- and third-order transverse shear deformation theory, Advanced Materials Research, 79-82 (2009), 1313-1316.

[14] T. Bailey, J.E. Hubbard: Distributed piezoelectric-polymer active vibration control of a cantilever beam, AIAA J. of Guidance, Control, and Dynamics 8 (1985), 605-611.

[15] I. Kreja, R. Schmidt: Large rotations in first-order shear deformation FE analysis of laminated shells, International Journal of Non-Linear Mechanics 41 (2006), 101-123.

[16] R. Schmidt, J.N. Reddy: A refined small strain and moderate rotation theory of elastic anisotropic shells, ASME Journal of Applied Mechanics 55 (1988), 611-617.

[17] I. Kreja, R. Schmidt, J.N. Reddy: Finite elements based on a first-order shear deformation moderate rotation shell theory with applications to the analysis of composite structures, Int. J. of Non-Linear Mechanics 32 (1997), 1123-1142.

[18] Q.D. Nguyen, S. Lentzen, R. Schmidt: A geometrically nonlinear third-order shear deformation finite plate element incorporating piezoelectric layers, Proc. 8th International Conference on Mechatronics Technology, ICMT 2004, Hanoi, Vietnam, 8 – 12 November 2004, eds. Nguyen Khoa Son, Pham Thuong Cat, Pham Anh Tuan, 303-308, Vietnam National University Publisher, Hanoi 2004.

[19] I. Kreja, R. Schmidt, Moderate rotation shell theory in FEM application. *Zeszyty Naukowe Politechniki Gdańskiej* (Research Transactions of Gdansk University of Technology), 522 (1995), 229-249.